DOI: 10.1021/ic900977m

Inorganic Chemistry
Article

Structures and Spin States of Bis(tridentate)-Type Mononuclear and Triple Helicate Dinuclear Iron(II) Complexes of Imidazole-4-carbaldehyde azine

Yukinari Sunatsuki,*,† Ryohei Kawamoto,† Kunihiro Fujita,† Hisashi Maruyama,† Takayoshi Suzuki,† Hiroyuki Ishida,† Masaaki Kojima,*,† Seiichiro Iijima,‡ and Naohide Matsumoto§

†*Department of Chemistry, Faculty of Science, Okayama University, Tsushima-naka 3-1-1, Okayama 700-8530, Japan,* ‡*National Institute of Advanced Industrial Science and Technology, Tsukuba 305-8566, Japan, and* §*Department of Chemistry, Faculty of Science, Kumamoto University, Kurokami 2-39-1, Kumamoto 860-8555, Japan*

Received May 19, 2009

Mononuclear $[Fe(H_2L^R)_2]^{2+}$ and dinuclear $[Fe_2(H_2L^R)_3]^{4+}$ (R = H, 2-Me, 5-Me) complexes containing the new imidazole-4-carbaldehyde azine ligand (H_2L^H) and its derivatives ($H_2L^{2\text{-Me}}$ and $H_2L^{5\text{-Me}}$) prepared from the condensation reaction of 4-formylimidazole or 2-methyl- or 5-methyl-4-formylimidazole with hydrazine (2:1) were prepared, and their magnetostructural relationships were studied. In the mononuclear complexes, H_2L^R acts as an unsymmetrical tridentate ligand with two imidazole nitrogen atoms and one azine nitrogen atom, while in the dinuclear complexes, H_2L^R acts as a dinucleating ligand employing four nitrogen atoms to form a triple helicate. At room temperature, $[Fe_2(H_2L^H)_3](ClO_4)_4$ and $[Fe_2(H_2L^{2\text{-Me}})_3](ClO_4)_4$ were in the high-spin (HS) and low-spin (LS) states, respectively. The results are in accordance with the ligand field strength of $H_2L^{2\text{-Me}}$ with electron-donating methyl groups being stronger than H_2L^H, with the order of the ligand field strengths being $H_2L^{2\text{-Me}} > H_2L^H$. However, in the mononuclear $[Fe(H_2L^H)_2](ClO_4)_2$ and $[Fe(H_2L^{2\text{-Me}})_2](ClO_4)_2$ complexes, a different order of ligand field strengths, $H_2L^H > H_2L^{2\text{-Me}}$, was observed because $[Fe(H_2L^H)_2](ClO_4)_2$ was in the LS state while $[Fe(H_2L^{2\text{-Me}})_2](ClO_4)_2$ was in the HS state at room temperature. X-ray structural studies revealed that the interligand steric repulsion between a methyl group of an $H_2L^{2\text{-Me}}$ ligand and the other ligand in $[Fe(H_2L^{2\text{-Me}})_2](ClO_4)_2$ is responsible for the observed change in the spin state. Two kinds of crystals, needles and blocks, were isolated for $[Fe_2(H_2L^H)_3](BF_4)_4$, and both exhibited a sharp spin transition, [LS−HS] ↔ [HS−HS]. The spin transition of the block crystals is more abrupt with a hysteresis, $T_c\uparrow$ = 190 K and $T_c\downarrow$ = 183 K with ΔT = 7 K.

Introduction

Increasing attention is being paid to bistable molecules because they can be used as molecular memories and switches in electronic devices.[1] The phenomenon of spin-crossover (SCO) between the low-spin (LS) and high-spin (HS) states, which is observed in some octahedral $3d^n$ ($4 \le n \le 7$) metal complexes, is the most spectacular example of molecular bistability. SCO can be brought about by external perturbations such as variation in the temperature or pressure, or by counterions or even solvent molecule exchange, light irradiation, a magnetic field, or soft or hard X-ray irradiation.[2]

Busch and Stratton reported in papers in 1958 and 1960 that the 2-pyridinealdazine (= bis(pyridylimine)) ligand, PAA (Scheme 1), could form two types of metal complexes, $[M(PAA)_2]^{2+}$ (M^{II} = Fe, Ni) and $[M_2(PAA)_3]^{4+}$ (see Scheme 2).[3] In the former mononuclear complex, PAA acts as an unsymmetrical tridentate ligand with two pyridyl nitrogen atoms and one azine nitrogen atom. In the latter complex, PAA was assumed to act as a dinucleating ligand employing all four nitrogen atoms. The workers recognized that the dinuclear species must consist of three strands

*To whom correspondence should be addressed. E-mail: sunatuki@cc.okayama-u.ac.jp (Y.S.), kojima@cc.okayama-u.ac.jp (M.K.).

(1) (a) Kahn, O.; Martinez, J. C. *Science* **1998**, *279*, 44–48. (b) Hayami, S.; Danjobara, K.; Inoue, K.; Ogawa, Y.; Matsumoto, N.; Maeda, Y. *Adv. Mater.* **2004**, *16*, 869–872. (c) Létard, J. F.; Guionneau, P.; Goux-Capes, L. *Spin Crossover in Transition Metal Compounds*; Gütlich, P., Goodwin, H. A., Eds.; *Top. Curr. Chem.*; Vol. *235*, p 221.(d) Niel, V.; Martinez-Agudo, J. M.; Muoz, M. C.; Gaspar, A. B.; Real, J. A. *Inorg. Chem.* **2001**, *40*, 3838–3839.

(2) (a) König, E. *Prog. Inorg. Chem.* **1987**, *35*, 527–623. (b) König, E. *Struct. Bonding* (*Berlin*) **1991**, *76*, 51–152. (c) Goodwin, H. A. *Coord. Chem. Rev.* **1976**, *18*, 293–325. (d) Gütlich, P.; Hauser, A.; Spiering, H. *Angew. Chem., Int. Ed. Engl.* **1994**, *33*, 2024–2054. (e) Real, J. A.; Gaspar, A. B.; Niel, V.; Muñoz, M. C. *Coord. Chem. Rev.* **2003**, *236*, 121–141. (f) Lemercier, G.; Verelst, M.; Bousseksou, A.; Varret, F.; Tuchagues, J.-P. In *Magnetism: A Supramolecular Function*, NATO ASI Series, Series C 484; Kahn O., Ed.; Kluwer Academic Publ.: Dordrecht, The Netherlands, 1996; pp 335−356. (g) Gütlich, P.; Garcia, Y.; Woike, T. *Coord. Chem. Rev.* **2001**, *219*−*221*, 839–879. (h) *Spin Crossover in Transition Metal Compounds*; Gütlich, P., Goodwin, H. A., Eds.; *Top. Curr. Chem.*; Springer-Verlag: Berlin, 2004; Vols. *233*−*235*. (i) Real, J. A.; Gaspar, A. B.; Muñoz, M. C. *Dalton Trans.* **2005**, 2062–2079. (j) Vanko, G.; Renz, F.; Molnar, G.; Neisius, T.; Karpati, S. *Angew. Chem., Int. Ed.* **2007**, *46*, 5306–5309. (k) Bousseksou, A.; Negre, N.; Goiran, M.; Salmon, L.; Tuchagues, J.-P.; Boillot, M.-L.; Boukheddaden, K.; Varret, F. *Eur. Phys. J. B* **2000**, *13*, 451–456.

(3) (a) Stratton, W. J.; Busch, D. H. *J. Am. Chem. Soc.* **1958**, *80*, 1286–1289. (b) Stratton, W. J.; Busch, D. H. *J. Am. Chem. Soc.* **1958**, *80*, 3191–3195. (c) Stratton, W. J.; Busch, D. H. *J. Am. Chem. Soc.* **1960**, *82*, 4834–4839.

Published on Web 08/20/2009

Scheme 1. Ligands, PAA, H_2L^H, $H_2L^{2\text{-Me}}$, and $H_2L^{5\text{-Me}}$

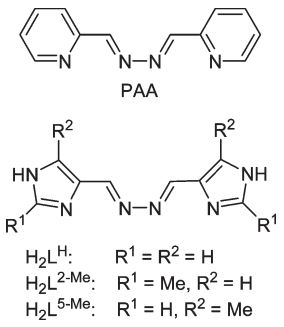

Scheme 2. Two Coordination Modes Adapted by PAA

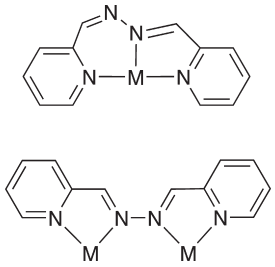

wrapped around two metals in a spiral fashion.[3,4] Both the iron(II) complexes, $[Fe(PAA)_2]^{2+}$ and $[Fe_2(PAA)_3]^{4+}$, were reported to be in the LS state.[3] An imidazole nitrogen atom usually exhibits a weaker ligand field strength than a pyridine nitrogen atom does,[5] and we expect that the imidazole analogue of PAA, H_2L^H, and its methyl derivatives, $H_2L^{2\text{-Me}}$ and $H_2L^{5\text{-Me}}$ (Scheme 1), will have the necessary ligand field strength to form SCO iron(II) complexes. The incorporation of imidazole groups has another advantage because the uncoordinated NH groups can be involved in hydrogen bond formation to increase cooperativity. For example, we have reported that Fe complexes with a tripodal ligand involving three imidazole groups have a 2-dimensional (2D) extended network structure based on imidazole−imidazolate hydrogen bonds and that they exhibit steep and multistep SCO behaviors.[5]

Dinuclear SCO Fe^{II} complexes have attracted attention because they can combine two properties like magnetic coupling and SCO in the same molecule, as well as the possibility of investigating new cooperative behavior.[6] In such complexes, the iron centers are coupled by intramolecular interactions, and three different spin-pair states, [LS−LS], [LS−HS], and [HS−HS], are possible. Actually, some complexes exhibit a two-step spin-crossover phenomenon, [LS−LS] ↔ "[LS−HS]" ↔ [HS−HS].[7,8] However, the half-SCO species, "[LS−HS]", can consist of either a 1:1 mixture of [LS−LS] and [HS−HS] complexes or a distinct [LS−HS] complex. Kaizaki and co-workers reported that the "[LS−HS]" species of their doubly pyrazolate-bridged two-step SCO diiron(II) complex is a mixture of [LS−LS] and [HS−HS] complexes.[8] Recently, Murray and co-workers confirmed for the first time the existence of the mixed spin state [LS−HS] from X-ray crystallographic data of the doubly 1,2,4-triazole-bridged complex.[9] Amoore et al. structurally characterized the three spin states, [LS−LS], [LS−HS], and [HS−HS], for the first time.[7g] Only a limited number of papers have dealt with dinuclear Fe^{II} SCO helicate complexes. Williams et al. have reported an Fe^{II} helicate involving benzimidazole ligands showing two-step SCO with negative cooperativity.[10] The Fe^{II}−imidazolimine complexes with a supramolecular triple-helicate structure exhibiting various SCO behaviors were also studied.[4,11] The SCO of this system was reinterpreted by Gütlich and co-workers.[12] Very recently, Pelleteret et al. reported LIESST (light-induced excited spin state trapping) in a dinuclear Fe^{II} helicate with ligands containing imidazolimine groups.[13]

Here we report the synthesis, characterization, structure, and magnetic properties of mononuclear $[Fe(H_2L^R)_2]^{2+}$ (R = H, 2-Me, 5-Me) and dinuclear $[Fe_2(H_2L^R)_3]^{4+}$ complexes, where H_2L^H, $H_2L^{2\text{-Me}}$, and $H_2L^{5\text{-Me}}$ denote imidazole-4-carbaldehyde azine, 2-methylimidazole-4-carbaldehyde azine, and 5-methylimidazole-4-carbaldehyde azine, respectively. Comparison of the SCO behaviors of the mononuclear complexes with those of the dinuclear triple-helicate complexes involving the same ligands is particularly important

(4) Hamblin, J.; Jackson, A.; Alcock, N. W.; Hannon, M. J. *J. Chem. Soc., Dalton Trans*. **2002**, 1635–1641.

(5) (a) Sunatsuki, Y.; Sakata, M.; Matsuzaki, S.; Matsumoto, N.; Kojima, M. *Chem. Lett*. **2001**, 1254–1255. (b) Sunatsuki, Y.; Ikuta, Y.; Matsumoto, N.; Ohta, H.; Kojima, M.; Iijima, S.; Hayami, S.; Maeda, Y.; Kaizaki, S.; Dahan, F.; Tuchagues, J.-P. *Angew. Chem., Int. Ed*. **2003**, *42*, 1614–1618. (c) Ohta, H.; Sunatsuki, Y.; Ikuta, Y.; Matsumoto, N.; Iijima, S.; Akashi, H.; Kambe, T.; Kojima, M. *Mater. Sci*. **2003**, *21*, 191–198. (d) Ikuta, Y.; Ooidemizu, M.; Yamahata, Y.; Yamada, M.; Osa, S.; Matsumoto, N.; Iijima, S.; Sunatsuki, Y.; Kojima, M.; Dahan, F.; Tuchagues, J.-P. *Inorg. Chem*. **2003**, *42*, 7001–7017. (e) Yamada, M.; Ooidemizu, M.; Ikuta, Y.; Osa, S.; Matsumoto, N.; Iijima, S.; Kojima, M.; Dahan, F.; Tuchagues, J.-P. *Inorg. Chem*. **2003**, *42*, 8406–8416. (f) Sunatsuki, Y.; Ohta, H.; Kojima, M.; Ikuta, Y.; Goto, Y.; Matsumoto, N.; Iijima, S.; Akashi, H.; Kaizaki, S.; Dahan, F.; Tuchagues, J.-P. *Inorg. Chem*. **2004**, *43*, 4154–4171. (g) Ohta, H.; Sunatsuki, Y.; Kojima, M.; Iijima, S.; Akashi, H.; Matsumoto, N. *Chem. Lett*. **2004**, *33*, 350–351. (h) Yamada, M.; Fukumoto, E.; Ooidemizu, M.; Bréfuel, N.; Matsumoto, N.; Iijima, S.; Kojima, M.; Re, N.; Dahan, F.; Tuchagues, J.-P. *Inorg. Chem*. **2005**, *44*, 6967–6974. (i) Yamada, M.; Hagiwara, H.; Torigoe, H.; Matsumoto, N.; Kojima, M.; Dahan, F.; Tuchagues, J.-P.; Re, N.; Iijima, S. *Chem.—Eur. J*. **2006**, *12*, 4536–4549. (j) Iijima, S.; Mizutani, F.; Niwa, O.; Matsumoto, N.; Sunatsuki, Y.; Kojima, M. *Hyperfine Interact*. **2007**, *166*, 397–402.

(6) Gaspar, A. B.; Muñoz, M. C.; Real, J. A. *J. Mater. Chem*. **2006**, *16*, 2522.

(7) (a) Ksenofontov, V.; Gasper, A. B.; Niel, V.; Reiman, S.; Real, J. A; Gütlich, P. *Chem.—Eur. J*. **2004**, *10*, 1291–1298. (b) Ortega-Villar, N.; Thompson, A. L.; Muñoz, M. C.; Ugalde-Saldivar, V. M.; Goeta, A. E.; Moreno-Esparza, R.; Real, J. A. *Chem.—Eur. J*. **2005**, *11*, 5721–5734. (c) Kitashima, R.; Imatomi, S.; Yamada, M.; Matsumoto, N.; Maeda, Y. *Chem. Lett*. **2005**, *34*, 1388–1389. (d) Real, J. A.; Bolvin, H.; Bousseksou, A.; Dworkin, A.; Kahn, O.; Varret, F.; Zarembowitch, J. *J. Am. Chem. Soc*. **1992**, *114*, 4650–4658. (e) Ksenofontov, V.; Spiering, H.; Reiman, S.; Garcia, Y.; Gaspar, A. B.; Moliner, N.; Real, J. A.; Gütlich, P. *Chem. Phys. Lett*. **2001**, *348*, 381–386. (f) Murray, K. S. *Eur. J. Inorg. Chem*. **2008**, 3101–3121. (g) Amoore, J. J.; Kepert, C. J.; Cashion, J. D.; Moubaraki, B.; Neville, S. M.; Murray, K. S. *Chem.—Eur. J*. **2006**, *12*, 8220–8227. (h) Ruben, M. R.; Ziener, U.; Lehn, J.-M.; Ksenofontov, V.; Gütlich, P.; Vaughan, G. B. M. *Chem.—Eur. J*. **2005**, *11*, 94–100. (i) Ruben, M.; Rojo, J.; Romero-Salguero, F. J.; Uppadine, L. H.; Lehn, J.-M. *Angew. Chem., Int. Ed*. **2004**, *43*, 3644–3662.

(8) Nakano, K.; Kawata, S.; Yoneda, K.; Fuyuhiro, A.; Yagi, T.; Nasu, S.; Morimoto, S.; Kaizaki, S. *Chem. Commun*. **2004**, 2892–2893.

(9) Klingele, M.; Moubaraki, B.; Cashion, J. D.; Murray, K. S.; Brooker, S. *Chem. Commun*. **2005**, 987–988.

(10) (a) Telfer, S. G.; Bocquet, B.; Williams, A. F. *Inorg. Chem*. **2001**, *40*, 4818–4820. (b) Charbonniere, L. J.; Williams, A. F.; Piguet, C.; Bernardinelli, G.; Rivara-Minten, E. *Chem.—Eur. J*. **1998**, *4*, 485–493.

(11) Tuna, F.; Lees, M. R.; Clarkson, G. J.; Hannon, M. J. *Chem.—Eur. J*. **2004**, *10*, 5737–5750.

(12) Garcia, Y.; Grunert, C. M.; Reiman, S.; van Campenhoudt, O.; Gütlich, P. *Eur. J. Inorg. Chem*. **2006**, 3333–3339.

(13) Pelleteret, D.; Clérac, R.; Mathonière, C.; Harté, E.; Schmitt, W.; Kruger, P. E. *Chem. Commun*. **2009**, 221–223.

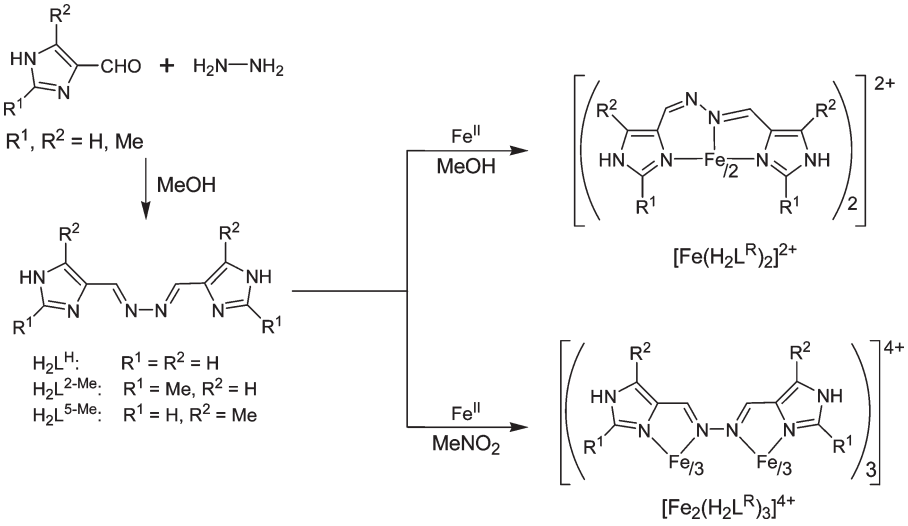

Figure 1. Synthetic procedures yielding the H_2L^R (R = H, 2-Me, 5-Me) ligands and the mononuclear and dinuclear Fe^{II} complexes.

in studying the structural effects. Part of this work has been communicated previously.[14]

Results and Discussion

Synthesis and Characterization. The synthetic procedures yielding the H_2L^R (R = H, 2-Me, 5-Me) ligands and the Fe^{II} complexes are shown schematically in Figure 1. The ligands were prepared by condensation of 4-formylimidazole, or its derivatives, 2-methyl- or 5-methyl-4-formylimidazole, with hydrazine in a 2:1 mol ratio in methanol. Although the ligands are sparingly soluble in common solvents, they react with an Fe^{II} ion. The mononuclear complex, $[Fe(H_2L^H)_2](ClO_4)_2 \cdot MeOH$ (**1H·ClO$_4$**), was prepared by reaction of H_2L^H and $Fe(ClO_4)_2 \cdot 6H_2O$ in a 2:1 mol ratio in methanol. The color of the mixture changed from orange to dark purple as the reaction proceeded, and on addition of diethyl ether, the perchlorate of **1H**, $[Fe(H_2L^H)_2](ClO_4)_2 \cdot MeOH$ (**1H·ClO$_4$**), was isolated as dark purple crystals. A similar color change from red to blue was reported during the preparation of $[Fe(PAA)_2]^{2+}$. The helical $[Fe_2(PAA)_3]^{4+}$ complex, which formed first, underwent exchange reactions on heating or standing in methanol to form the mononuclear complex $[Fe(PAA)_2]^{2+}$.[3,15] Thus, **1H** is suggested to form by way of the dinuclear complex, $[Fe_2(H_2L^H)_3]^{4+}$ (**2H**). The corresponding 2-methyl and 5-methyl derivatives, $[Fe(H_2L^{2\text{-}Me})_2](ClO_4)_2 \cdot H_2O$ (**1Me·ClO$_4$**) and $[Fe(H_2L^{5\text{-}Me})_2](ClO_4)_2 \cdot 1.5H_2O$ (**1Me′·ClO$_4$**), were prepared in a similar manner and isolated as reddish orange crystals and dark purple crystals, respectively. The distinct color difference, dark purple (**1H**, **1Me′**) versus reddish orange (**1Me**), suggested that the complexes were in different spin states. The dinuclear complexes, $[Fe_2(H_2L^H)_3](ClO_4)_4$ (**2H·ClO$_4$**), $[Fe_2(H_2L^{2\text{-}Me})_3](ClO_4)_4$ (**2Me·ClO$_4$**), and $[Fe_2(H_2L^{5\text{-}Me})_3](ClO_4)_4$ (**2Me′·ClO$_4$**) were prepared by reaction of the respective ligand and $Fe(ClO_4)_2 \cdot 6H_2O$ in nitromethane in a 3:2 mol ratio. Once again, the colors of the compounds were different: orange (**2H·ClO$_4$**) and reddish or dark brown (**2Me·ClO$_4$**). The dinuclear complexes are stable only in such solvents as nitromethane and acetonitrile. The instability of the complexes in such solvents as methanol and *N,N*-dimethylformamide may be related to the coordinating ability of these solvent molecules. Because of this instability, it was difficult to exchange the counterions of the dinuclear complexes. The $[Fe_2(H_2L^H)_3](BF_4)_4$ (**2H·BF$_4$**) complex, prepared by reaction of $Fe(BF_4)_2 \cdot 6H_2O$ and H_2L^H in nitromethane, was isolated in two kinds of crystals, needles and blocks, on crystallization from nitromethane by slow diffusion of diethyl ether. The crystals were separated manually under a microscope. Crystal solvents of the samples of **2H·BF$_4$** were easily lost on drying in vacuo, and such samples were used for magnetic studies.

The IR spectra of the H_2L^R (R = H, 2-Me, 5-Me) ligands showed strong characteristic absorptions at 1637−1639 cm^{-1}, assignable to the C=N stretching vibration.[16] The dinuclear complexes showed one ν(C=N) band in the 1617−1634 cm^{-1} region, while the mononuclear complexes showed two bands in the 1568−1594 and 1622−1630 cm^{-1} regions. The number of ν(C=N) bands, one for the dinuclear complexes and two for the mononuclear complexes, is in accordance with the symmetry of the complexes because in the mononuclear complexes the H_2L^R ligand functions as an unsymmetrical tridentate ligand. The ν(C=N) bands of the dinuclear complexes were not as sharp as those of the ligands and the mononuclear complexes, and this may be related to the fact that the two Fe^{II} sites are not equivalent (see below). The electron density in the C=N moiety is donated to a metal upon coordination, and the double bond character decreases and the position of the ν(C=N) band should shift to a lower wavenumber region. Thus, the bands in the lower wavenumber region of the mononuclear complexes (1568−1594 cm^{-1}) can be assigned to the coordinated C=N moiety. The bands in the higher wavenumber region (1622−1630 cm^{-1}) are observed near those of the free ligands (1637−1639 cm^{-1}), and they can

(14) Fujita, K.; Kawamoto, R.; Tsubouchi, R.; Sunatsuki, Y.; Kojima, M.; Iijima, S.; Matsumoto, N. *Chem. Lett.* **2007**, *36*, 1284–1285.
(15) Stratton, W. J.; Rettig, M. F.; Drury, R. F. *Inorg. Chim. Acta* **1969**, *3*, 97–102.
(16) Nakamoto, K. *Infrared and Raman Spectra of Inorganic and Coordination Compounds, Part B*, 5th ed.; John Wiley and Sons: New York, 1997.

Table 1. UV-vis Spectral Data of the H_2L^H Ligand in Methanol, and the Mononuclear (**1H**, **1Me**, **1Me′**) and the Dinuclear (**2H**, **2Me**, **2Me′**) Complexes in Acetonitrile at 295 K

complex	λ_{max}/nm (ε/M^{-1} cm^{-1})
$\mathbf{H_2L^H}$	205 (9300) 312 (33600)
1H	301(29700) 326 (25800) 343 (21900) 363 (sh, 6360) 557 (3840)
1Me	330 (64100) 488 (820)
1Me′	348 (35900) 410 (sh, 1380) 556 (4070)
2H	293 (56300) 463 (4790) 570 (sh, 830)
2Me	306 (61700) 467 (sh, 1100) 565 (sh, 180)
2Me′	319 (55200) 463 (sh, 4210) 570 (sh,1230)

be safely assigned to the uncoordinated C=N moiety. Close inspection of the positions of the lower wavenumber region bands reveals that **1H·ClO$_4$** (1588 cm^{-1}) and **1Me′·ClO$_4$** (1568 cm^{-1}) show the bands at lower energy than the **1Me·ClO$_4$** (1594 cm^{-1}). This difference can be explained in terms of the different spin states of these complexes. We have reported that the C=N vibration of the iron(II) complexes with a tripodal Schiff base ligand is sensitive to the spin state of iron; a complex in the LS state shows the band at a lower wavenumber than the HS complex.[1a] This trend holds for the present complexes: **1H·ClO$_4$** and **1Me′·ClO$_4$** are in the LS state, while **1Me·ClO$_4$** is in the HS state at room temperature (see below). IR spectroscopy has been used to study the spin states of other SCO Fe^{II} complexes.[17]

UV−vis spectral data of the mononuclear (**1H**, **1Me**, **1Me′**) and dinuclear (**2H**, **2Me**, **2Me′**) complexes in acetonitrile at 295 K are listed in Table 1. All complexes have an intense absorption band attributable to the metal-to-ligand charge-transfer (MLCT) transition in the visible region, which is responsible for the deep color, and thus weak d−d bands are obscured. The **1H** and **1Me′** complexes are in the LS state and show a strong absorption in the longer wavelength region (Figure 2). The **1Me** complex that is in the HS state shows a strong band in the shorter wavelength region (488 nm).[18] All complexes have an intense band at 293−350 nm assignable to the imine $\pi-\pi^*$ transition of the ligands.

The electrochemical properties of **1H** and **1Me** were studied by cyclic voltammetry (CV). The measurements were performed under nitrogen with a glassy carbon working electrode using an acetonitrile solution containing (n-Bu)$_4$NBF$_4$ (0.1 M) as supporting electrolyte. The redox couple ($Fe^{III/II}$) of **1H** appears at +0.291 V (E_{pc} = +0.256 V, E_{pa} = +0.325 V) versus Ag/Ag^+ irrespective of the scan rate ($10 \le \nu \le 200$ mV s^{-1}), the peak current ratio i_{pa}/i_{pc} was found to be 1.0, (i_{pa} or i_{pc})/$\nu^{1/2}$ was independent of ν, and the peak separation was 0.069 V (Figure 3). These results are consistent with an electrochemically reversible one-electron process; see eq 1.

$$[Fe^{III}(H_2L^H)]^{3+} + e^- \rightleftarrows [Fe^{II}(H_2L^H)]^{2+} \qquad (1)$$

The methyl derivative, **1Me**, shows the reversible $Fe^{III/II}$ redox couple at $E^{0\prime}$ = +0.444 V (E_{pc} = + 0.410 V, E_{pa} = + 0.478 V, ΔE_{pa} = 68 mV) versus Ag/Ag^+, which is more positive than that for **1H** by 0.153 V. In general, as the electron-donating ability of the substituent increases, the observed potential shifts in the cathodic (less positive) direction and the higher oxidation state of the metal is stabilized.[19] This implies that the substituent group directly affects the electron density present on the metal atom. The greater the electron density present on the metal atom as a result of the electron properties of the substituent group, the more difficult it should be to perform a reduction. Thus, replacement of hydrogen atoms with electron-donating methyl groups would make the compound easier to oxidize (i.e., the redox potential becomes less positive). The unexpected result that **1Me** is more difficult to oxidize than **1H** can be explained by the different spin states for **1Me** (HS) and **1H** (LS). Because a HS complex gives a weaker ligand field strength than a LS complex, the former becomes difficult to oxidize. The effect of the spin state on redox potential was pointed out for other Fe^{II} complexes.[20]

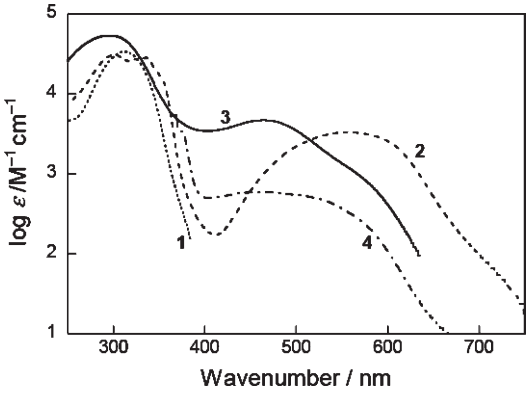

Figure 2. UV−vis spectra for the H_2L^H ligand (dotted line, **1**) in methanol, and mononuclear $[Fe(H_2L^H)]^{2+}$ (**1H**, dashed line, **2**), dinuclear $[Fe_2(H_2L^H)_3]^{4+}$ (**2H**, solid line, **3**) and mononuclear $[Fe(H_2L^{2\text{-}Me})]^{2+}$ (**1Me**, dashed-dotted line, **4**) in acetonitrile at 295 K.

CVs for the dinuclear complexes, **2H** and **2Me**, were measured under the same conditions as for the mononuclear complexes. The $Fe^{III/II}$ redox couple was irreversible for both complexes (Supporting Information, Figure S1). The anodic peak was observed at E_{pa} = +0.705 V for **2H** and at E_{pa} = +0.690 V for **2Me**, while the cathodic peak was not observed clearly for either complex. The less positive E_{pa} value for **2Me** is consistent with the presence of electron-donating methyl groups and its LS state. The irreversible nature may be related to instability of the dinuclear complexes in the Fe^{III} state.

Magnetic Properties of the Mononuclear Complexes. The magnetic behaviors of $[Fe(H_2L^H)_2](ClO_4)_2$ (**1H·ClO$_4$**) and $[Fe(H_2L^{2\text{-}Me})_2](ClO_4)_2$ (**1Me·ClO$_4$**) are shown in Figure 4 in the form of $\chi_M T$ versus T plots, where χ_M is the molar magnetic susceptibility and T is the absolute temperature. The mononuclear **1H·ClO$_4$** complex remains in the LS state over the range 5−300 K. The $\chi_M T$ value of 3.40 cm^3 K mol^{-1} of **1Me·ClO$_4$** at 300 K is within the range of expected values for a paramagnetic Fe^{II} in its

(17) (a) Herber, R. H.; Casson, L. M. *Inorg. Chem.* **1986**, *25*, 847–852. (b) Zilverentant, C L.; van Albada, G. A.; Bousseksou, A.; Haasnoot, J. G.; Reedijk, J. *Inorg. Chim. Acta* **2000**, *303*, 287–290.

(18) Levy, N. M.; Laranjeira, M. C.; Neves, A.; Franco, C. V. *J. Coord. Chem.* **1996**, *38*, 259−270.

(19) (a) Patterson, G. S.; Holm, R. H. *Inorg. Chem.* **1972**, *11*, 2285–2288. (b) Handy, R. F.; Lintvedt, R. L. *Inorg. Chem.* **1974**, *13*, 893–896. (c) Ma, G.; Kojima, M.; Fujita, J. *Bull. Chem. Soc. Jpn.* **1989**, *62*, 2547–2552.

(20) Hoselton, M. A.; Wilson, L. J.; Drago, R. S. *J. Am. Chem. Soc.* **1975**, *97*, 1722–1729.

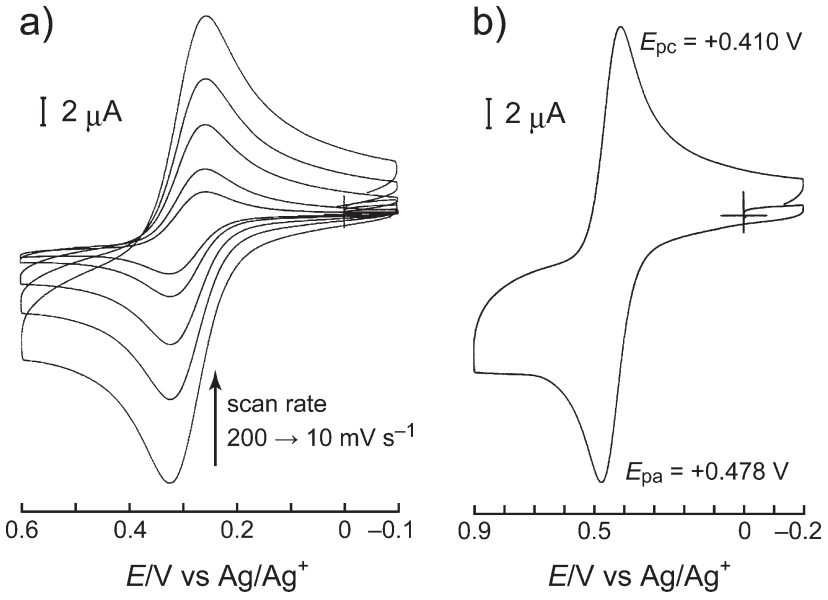

Figure 3. (a) Cyclic voltammograms of $[Fe(H_2L^{H})]^{2+}$ (**1H**) in acetonitrile containing 0.1 M $(n\text{-}Bu)_4NBF_4$ at a glassy carbon electrode as a function of the sweep rate: 10, 20, 50, 100, and 200 mV s^{-1}. (b) CV of $[Fe(H_2L^{2\text{-}Me})]^{2+}$ (**1Me**) under the same conditions as for (a) at 100 mV s^{-1}.

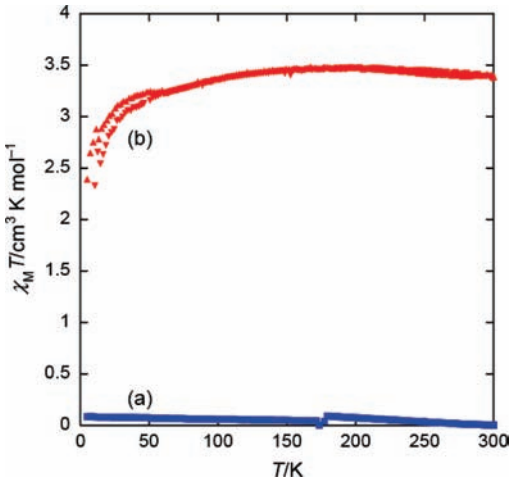

Figure 4. Magnetic behaviors of (a) $[Fe(H_2L^{H})_2](ClO_4)_2$ (**1H·ClO$_4$**) and (b) $[Fe(H_2L^{2\text{-}Me})_2](ClO_4)_2$ (**1Me·ClO$_4$**) in the form of $\chi_M T$ versus T plots. The samples were quickly cooled from 300 to 5 K, and χ_M was measured successively during heating (5−300 K, ▲) and cooling (300−5 K, ▼) modes, at a sweep rate of 2 K min^{-1}.

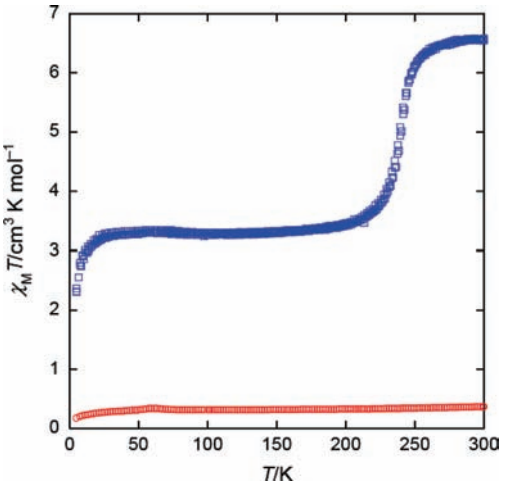

Figure 5. Magnetic behaviors of $[Fe_2(H_2L^{H})_3](ClO_4)_4$ (**2H·ClO$_4$**, blue) and $[Fe_2(H_2L^{2\text{-}Me})_3](ClO_4)_4$ (**2Me·ClO$_4$**, red) in the form of a $\chi_M T$ versus T plot.

HS state with some orbital contributions. The drop of $\chi_M T$ below 50 K may be a combined effect of SCO and zero-field splitting (ZFS) of Fe^{II} in the HS state. The magnetic measurements clearly indicate that **1H·ClO$_4$** and **1Me·ClO$_4$** are in the LS and HS states, respectively, at least above 50 K. These results are unexpected, because the ligand field strength of the $H_2L^{2\text{-}Me}$ ligand will be larger than that of the H_2L^{H} ligand because of the presence of electron-donating methyl groups, and **1Me·ClO$_4$** is expected to be in the LS state. The reason for **1Me·ClO$_4$** being in the HS state can be explained in terms of intramolecular steric repulsion between a methyl group of an $H_2L^{2\text{-}Me}$ ligand and the other ligand in the complex (see later). The $[Fe(H_2L^{5\text{-}Me})_2](ClO_4)_2$ (**1Me′·ClO$_4$**) complex does not involve such a steric congestion, and the $\chi_M T$ value stays at almost 0 cm^3 K mol^{-1} over the whole temperature range demonstrating the LS state. The substituent effect on the spin equilibrium was also observed for Fe^{II} complexes with hexadentate ligands.[20]

Magnetic Properties of the Dinuclear Complexes. The magnetic behaviors of $[Fe_2(H_2L^{H})_3](ClO_4)_4$ (**2H·ClO$_4$**) and $[Fe_2(H_2L^{2\text{-}Me})_3](ClO_4)_4$ (**2Me·ClO$_4$**) are shown in Figure 5 in the form of a $\chi_M T$ versus T plot. Complex **2Me·ClO$_4$** stayed in the LS state over the entire temperature range, and this result is in accordance with the strong ligand field strength of the $H_2L^{2\text{-}Me}$ ligand caused by the presence of electron-donating methyl groups. Complex **2H·ClO$_4$** exhibited an abrupt SCO behavior at about 240 K. Above 250 K, the $\chi_M T$ value was nearly constant at 6.6 cm^3 K mol^{-1}, which is close to the calculated spin-only value for the magnetically uncoupled [HS−HS] system ($\chi_M T$ = 6.0 cm^3 K mol^{-1}). In the temperature range 30−220 K, the value of $\chi_M T$ was nearly constant at 3.3 cm^3 K mol^{-1}, indicating that 50% of the Fe^{II} sites were in the HS state. The half-SCO state was trapped, the

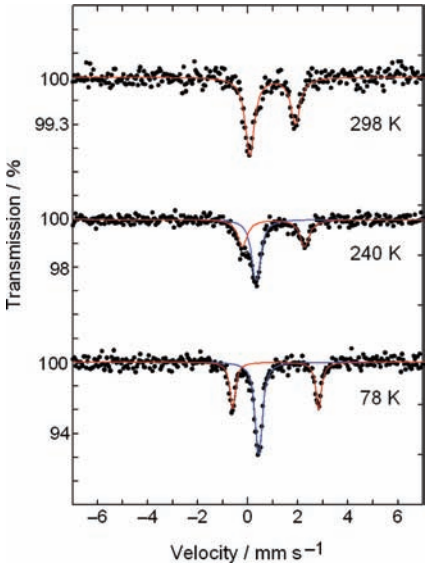

Figure 6. Mössbauer spectra for $[Fe_2(H_2L^H)_3](ClO_4)_4$ (**2H·ClO$_4$**) at 78, 240, and 298 K.

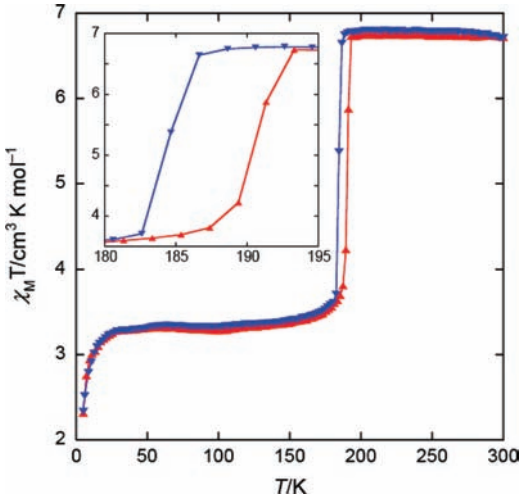

Figure 7. Magnetic behavior of the block crystals of $[Fe_2(H_2L^H)_3](BF_4)_4$ (**2H·BF$_4$**) in the form of $\chi_M T$ versus T plots. A hysteresis (inset) is observed; $T_c\uparrow$ = 190 K and $T_c\downarrow$ = 183 K with ΔT = 7 K.

complex was locked into it, and it did not change into the [LS−LS] state on further cooling. The decrease in $\chi_M T$ observed below about 20 K is probably due to the ZFS effect.[11] Three different spin-pair states are possible in diiron(II) complexes: [LS−LS], [LS−HS], and [HS−HS]. Actually, some complexes exhibit a two-step spin-crossover phenomenon, [LS−LS] ↔ "[LS−HS]" ↔ [HS−HS].[7,8] The half-SCO species, "[LS−HS]", can consist of either a 1:1 mixture of [LS−LS] and [HS−HS] complexes or a distinct [LS−HS] complex. That the half-SCO species of $[Fe_2(H_2L^H)_3](ClO_4)_4$ has a mixed-spin state, [LS−HS], was verified by X-ray crystal structure analysis (see later).

The temperature dependence of Mössbauer spectra of **2H·ClO$_4$** agrees with the magnetic susceptibility results. At 298 K, the Mössbauer spectrum consists of a single quadrupole doublet (δ = 0.99 mm s^{-1}, ΔE_Q = 1.82 mm s^{-1}), demonstrating the sole existence of HS Fe^{II} (Supporting Information, Table S1 and Figure 6). We noticed that the bands were broad, with a full width at half-height of Γ = 0.44 mm s^{-1}. This suggests that the Fe^{II} sites are not equivalent. At 78 K, the spectrum consists of two doublets exhibiting quadrupole splitting (HS Fe^{II}, δ = 1.11 mm s^{-1}, ΔE_Q = 3.44 mm s^{-1}, and Γ = 0.26 mm s^{-1}; LS Fe^{II}, δ = 0.44 mm s^{-1}, ΔE_Q = 0.12 mm s^{-1}, and Γ = 0.29 mm s^{-1}). Deconvolution of the spectrum at 78 K revealed the mole fraction of the HS Fe^{II} species to be 44%. These results agree with the magnetic susceptibility results.

As described above, $[Fe_2(H_2L^H)_3](BF_4)_4$ (**2H·BF$_4$**) was obtained in two kinds of crystals, needles and blocks, and they exhibited different SCO behaviors. The needles showed an abrupt spin transition at 254 K (Supporting Information, Figure S2) with behavior similar to that of **2H·ClO$_4$**. The block crystals exhibited a more abrupt spin transition at about 190 K accompanied by a hysteresis, $T_c\uparrow$ = 190 K and $T_c\downarrow$ = 183 K with ΔT = 7 K (Figure 7). The correlation between the structure and magnetic properties of the two forms of **2H·BF$_4$** will be discussed later in the section concerning X-ray structures.

Differential scanning calorimetric (DSC) measurements of the two crystal forms of **2H·BF$_4$** were carried out in the 120−280 K temperature range at a rate of 5 K min^{-1}. The temperature dependence of heat flow during heating and cooling for the two samples is shown in Supporting Information, Figure S3. Anomalies in the heat flow for needle crystals appear during heating at $T_c\uparrow$ = 258.0 K and $T_c\downarrow$ = 257.2 K during cooling. These values agree reasonably well with those observed from the $\chi_M T$ versus T plot. The overall enthalpy (ΔH) and entropy (ΔS) variations associated with the SCO determined from the DSC curves are ΔH = 5.6 ± 0.4 kJ mol^{-1} and ΔS = 21.7 ± 1.6 J K^{-1} mol^{-1} for the heating mode, and ΔH = −6.14 ± 0.13 kJ mol^{-1} and ΔS = −23.9 ± 0.5 J K^{-1} mol^{-1} for the cooling mode. The block crystals exhibited anomalies in the heat flow at $T_c\uparrow$ = 188.7 K and $T_c\downarrow$ = 182.4 K, which match reasonably well with the magnetic data. A shoulder observed in the heating mode may be due to the presence of an impurity. The thermodynamic parameters are ΔH = 9.0 ± 0.4 kJ mol^{-1} and ΔS = 48 ± 2 J K^{-1} mol^{-1} for the heating mode, and ΔH = −9.39 ± 0.10 kJ mol^{-1} and ΔS = −51.5 ± 0.5 J K^{-1} mol^{-1} for the cooling mode.

The $[Fe_2(H_2L^{5\text{-Me}})_3](ClO_4)_4$ (**2Me′·ClO$_4$**) complex was in the LS state over the temperature range 5−300 K. This result indicates that the $H_2L^{5\text{-Me}}$ ligand exerts a stronger ligand field strength than the H_2L^H ligand because of the presence of electron-donating methyl groups.

X-ray Crystal Structures

Structure of the $H_2L^{2\text{-Me}}$ Ligand. Crystals of $H_2L^{2\text{-Me}}$ suitable for X-ray crystal structure analysis were grown from a methanol solution in a refrigerator. The ligand crystallizes in the space group *Pbca* (No. 61) with Z = 4. The crystallographic data are collated in Table 2, and selected bond lengths and angles are listed in Supporting Information, Table S2. Figure 8 shows an Oak Ridge Thermal Ellipsoid Plot (ORTEP) drawing with atom numbering scheme. There is a crystallographic inversion center at the midpoint of N(3) and N(3)^i. The molecule is the *E*-*E* isomer. The nitrogen−nitrogen bond N(3)−N(3)^i (1.409(3) Å) can be formally defined as a single bond and compares closely with the N−N bond distance in

Table 2. X-ray Crystallographic Data for $H_2L^{2\text{-Me}}$, $[Fe(H_2L^{H})_2](ClO_4)_2\cdot 2CH_3CN$ (**1H·ClO$_4$**), $[Fe(H_2L^{2\text{-Me}})_2](ClO_4)_2\cdot 1.6CH_3CN$ (**1Me·ClO$_4$**), $[Fe(H_2L^{5\text{-Me}})_2](ClO_4)_2\cdot H_2O$ (**1Me′·ClO$_4$**), $[Fe_2(H_2L^{H})_3](ClO_4)_4\cdot 5CH_3NO_2$ (**2H·ClO$_4$**), $[Fe_2(H_2L^{2\text{-Me}})_3](ClO_4)_4$ (**2Me·ClO$_4$**), and $[Fe_2(H_2L^{H})_3](BF_4)_4\cdot 7CH_3NO_2$ (**2H·BF$_4$**)

	$H_2L^{2\text{-Me}}$	**1H·ClO$_4$**	**1Me·ClO$_4$**	**1Me′·ClO$_4$**
formula	$C_{10}H_{12}N_6$	$C_{20}H_{22}Cl_2FeN_{14}O_8$	$C_{116}H_{144}Cl_{10}Fe_5N_{68}O_{40}$	$C_{20}H_{26}Cl_2FeN_{12}O_9$
formula weight	216.24	713.24	3764.61	705.25
crystal system	orthorhombic	monoclinic	tetragonal	monoclinic
space group	*Pbca* (No. 61)	$P2_1/n$ (No. 14)	$I4_1/a$ (No. 88)	$P2_1/n$ (No. 14)
a/Å	9.5559(17)	11.2951(6)	22.8537(12)	9.40352(19)
b/Å	8.0270(11)	13.0064(5)	22.8537(12)	25.7816(7)
c/Å	14.798(3)	19.6897(7)	31.4028(15)	11.7835(4)
α/deg	90	90	90	90
β/deg	90	98.1490(17)	90	97.9137(11)
γ/deg	90	90	90	90
V/Å^3	1135.1(3)	2863.4(2)	16401.4(13)	2829.56(13)
T/K	293	103	200	163
Z	4	4	4	4
D_{calc}/g cm^{-3}	1.265	1.654	1.524	1.655
μ/cm^{-1}	0.847	7.849	6.892	7.936
$R_1{}^a$ [$I > 2\sigma(I)$]	0.0721	0.0414	0.0720	0.0493
$wR_2{}^b$ [all data]	0.2623	0.1075	0.2060	0.1311

	2H·ClO$_4$		**2Me·ClO$_4$**	**2H·BF$_4$**
formula	$C_{29}H_{39}Cl_4Fe_2N_{23}O_{26}$		$C_{30}H_{36}Cl_4Fe_2N_{18}O_{16}$	$C_{61}H_{89}B_8F_{32}Fe_4N_{49}O_{27}$
formula weight	1379.27		1158.23	2858.49
crystal system	monoclinic		trigonal	triclinic
space group	$P2_1/c$ (No. 14)		$P\bar{3}c1$ (No. 165)	$P\bar{1}$ (No. 2)
a/Å	16.1920(5)	16.0009(10)	10.031(2)	11.5903(7)
b/Å	17.7330(4)	17.2727(10)	10.031(2)	15.5367(10)
c/Å	19.9849(6)	19.8102(11)	24.859(6)	17.4994(10)
α/deg	90		90	90.2947(18)
β/deg	102.1350(12)	102.5478(19)	90	90.2919(18)
γ/deg	90		120	108.5083(18)
V/Å^3	5610.1(3)	5344.3(5)	2166.2(9)	2988.1(3)
T/K	293	103	93	173
Z	4		2	1
D_{calc}/g cm^{-3}	1.633	1.714	1.776	1.588
μ/cm^{-1}	8.081	8.482	10.082	6.104
$R_1{}^a$ [$I > 2\sigma(I)$]	0.0557	0.0649	0.0393	0.0682
$wR_2{}^b$ [all data]	0.1657	0.1736	0.1188	0.2158

$^a R_1 = \sum||F_o| - |F_c||/\sum|F_o|$. $^b wR_2 = [\sum w(|F_o^2| - |F_c^2|)^2/\sum w|F_o^2|^2]^{1/2}$.

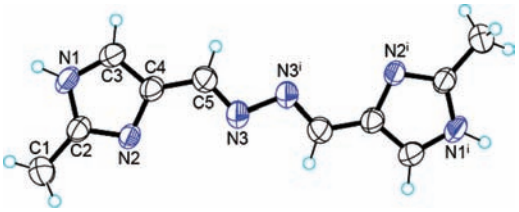

Figure 8. X-ray molecular structure of the $H_2L^{2\text{-Me}}$ ligand with atom numbering scheme. The superscript i denotes the atoms generated by symmetry operation with operator of $1-x, -y, -z$.

hydrazine (1.45 Å). The C−N bond C(5)−N(3) (1.278(4) Å) is considered to have full double-bond character. Supporting Information, Figures S4 and S5 show the packing diagrams. Imidazole N(1)−H(4) is hydrogen bonded to N(2) of the neighboring molecule, N(1)−H(4)···N(2) 2.845(3) Å, to form a 2D sheet structure in the *ac*-plane (Supporting Information, Figure S4). The imidazole groups in the neighboring sheets are linked by $\pi-\pi$ stacking interactions (3.53 Å) to form a 3D structure (Supporting Information, Figure S5).

Structure of $[Fe(H_2L^{H})_2](ClO_4)_2\cdot 2CH_3CN$ (1H·ClO$_4$). The crystal structure of **1H·ClO$_4$**, which crystallizes in the space group $P2_1/n$ (No. 14) with $Z = 4$, was determined at 103 K. The asymmetric unit consists of one $[Fe(H_2L^{H})_2]^{2+}$ cation, two ClO_4^- anions, and two acetonitrile molecules. An ORTEP drawing of **1H·ClO$_4$** is shown in Figure 9. The Fe^{II} ion binds two H_2L^{H} ligands and has a pseudo-octahedral coordination geometry. Each ligand in the *Z*-*E* configuration serves as a tridentate ligand and coordinates meridionally to the metal ion with two imidazole nitrogen atoms and one azine nitrogen atom, and the other azine nitrogen atom remains uncoordinated (Scheme 2).[21] Thus, the H_2L^{H} ligand becomes unsymmetrical upon coordination to form a five-membered and a six-membered chelate. This creates disorder in the moieties involving azine: C(4)−N(3)−N(4)−C(5) (Occ = 0.56) and C(6)−N(5)−N(6)−C(7) (Occ = 0.44), and C(14)−N(11)−N(12)−C(15) (Occ = 0.78) and C(16)−N(13)−N(14)−C(17) (Occ = 0.22). Selected bond lengths and angles are listed in Table 3. All of the Fe−N coordinate bond distances (1.950(2)−2.021(12) Å) are typical for LS Fe^{II} in accordance with the magnetic study.[22] The crystal structure is shown in Supporting Information, Figure S6. Two imidazole hydrogen atoms, N(8)−H(9) and N(9)−H(12), are linked to O(6) and O(5), respectively, of a ClO_4 ion, by hydrogen bonds with

(21) Karmakar, R.; Choudhury, C. R.; Batten, S. R.; Mitta, S. *J. Mol. Struct.* **2007**, *826*, 75–81.
(22) Beattie, J. K. *Adv. Inorg. Chem.* **1988**, *32*, 1–53.

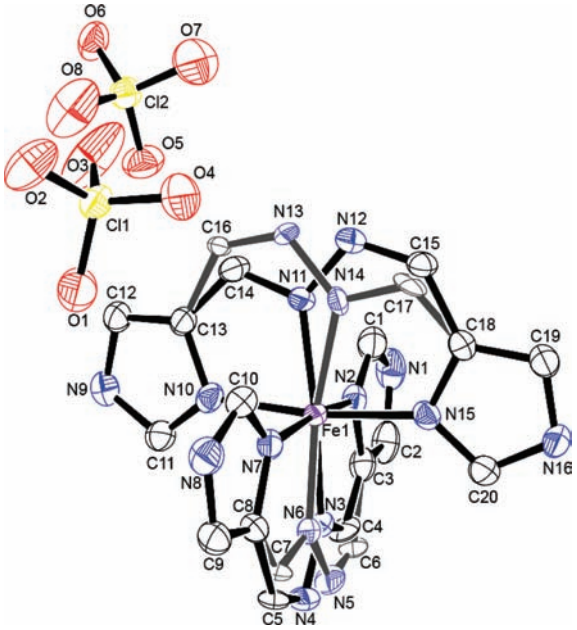

Figure 9. X-ray molecular structure of $[Fe(H_2L^H)_2](ClO_4)_2 \cdot 2CH_3CN$ (**1H·ClO$_4$**) with an atom numbering scheme showing the 50% probability ellipsoids. The hydrogen atoms and acetonitrile molecules have been omitted for clarity. Color code: purple, LS Fe; blue, N; black, C; yellow, Cl; and red, O. The structure suffers from disorder at the azine moieties.

Table 3. Relevant Bond Lengths (Å) and Angles (deg) with Their Estimated Standard Deviations in Parentheses for $[Fe(H_2L^H)_2](ClO_4)_2 \cdot 2CH_3CN$ (**1H·ClO$_4$**)

Bond Distances/Å			
Fe(1)−N(2)	1.950(2)	Fe(1)−N(10)	1.979(2)
Fe(1)−N(3)	1.992(5)	Fe(1)−N(11)	1.975(3)
Fe(1)−N(6)	1.973(6)	Fe(1)−N(14)	2.021(12)
Fe(1)−N(7)	1.951(2)	Fe(1)−N(15)	1.9656(19)
Bond Angles/deg			
N(2)−Fe(1)−N(3)	78.13(17)	N(6)−Fe(1)−N(7)	77.0(2)
N(2)−Fe(1)−N(6)	95.9(2)	N(6)−Fe(1)−N(10)	94.31(19)
N(2)−Fe(1)−N(7)	172.73(9)	N(6)−Fe(1)−N(11)	167.2(2)
N(2)−Fe(1)−N(10)	87.73(9)	N(6)−Fe(1)−N(14)	162.5(3)
N(2)−Fe(1)−N(11)	95.08(11)	N(6)−Fe(1)−N(15)	93.56(19)
N(2)−Fe(1)−N(14)	96.2(3)	N(7)−Fe(1)−N(10)	91.29(8)
N(2)−Fe(1)−N(15)	89.81(8)	N(7)−Fe(1)−N(11)	91.83(11)
N(3)−Fe(1)−N(7)	94.75(17)	N(7)−Fe(1)−N(14)	91.1(3)
N(3)−Fe(1)−N(10)	93.50(15)	N(7)−Fe(1)−N(15)	92.10(8)
N(3)−Fe(1)−N(11)	170.62(18)	N(10)−Fe(1)−N(11)	79.65(11)
N(3)−Fe(1)−N(14)	166.2(3)	N(10)−Fe(1)−N(14)	98.9(3)
N(3)−Fe(1)−N(15)	93.48(15)	N(10)−Fe(1)−N(15)	171.96(8)
		N(11)−Fe(1)−N(15)	92.96(11)
		N(14)−Fe(1)−N(15)	73.8(3)

distances of N(8)···O(6) = 3.006(3) and N(9)···O(5) = 2.889(3) Å, and N(16)−H(19) is linked to the azine N(4) atom with a distance of N(16)···N(4) = 2.969(4) Å. Because the azine moiety is disordered, there are two situations. When N(3) and N(4) atoms exist, a 2D sheet is formed in the *ab*-plane, while there is a 1D chain when N(5) and N(6) atoms exist instead of N(3) and N(4). The last imidazole hydrogen atom, N(1)−H(2), is linked to O(2) of ClO_4^- by a hydrogen bond with a distance of N(1)···O(2) = 2.935(3) Å. However, it does not participate in forming dimensionality. The imidazole N(8)−H(9) hydrogen atom is also hydrogen bonded to N(17) of acetonitrile with a distance of N(8)···N(17) = 3.131(4) Å, which also does not participate in forming dimensionality.

Structure of $[Fe(H_2L^{2\text{-}Me})_2](ClO_4)_2 \cdot 1.6CH_3CN$ (1Me·ClO$_4$). Magnetic studies revealed that **1Me·ClO$_4$** stays in the HS state over the 5−300 K temperature range, and the crystal structure was determined at 200 K by the X-ray diffraction method. The complex crystallizes in the space group $I4_1/a$ (No. 88). The asymmetric unit consists of 1.25 $[Fe(H_2L^{2\text{-}Me})_2]^{2+}$, 2.5 ClO_4^- anions, and two acetonitrile molecules. As Supporting Information, Figure S7 shows, there are two complex cations involving Fe(1) and Fe(2) in the crystal. The overall molecular structure is similar to that of **1H·ClO$_4$**. In either complex cation, one of the two $H_2L^{2\text{-}Me}$ ligands suffers from disorder in the azine moiety. In the complex containing Fe(1), the Occ values for C(15)−N(9)−N(10)−C(16) and C(17)−N(11)−N(12)−C(18) were 0.53 and 0.47, respectively, while in the other complex containing Fe(2), both Occ values for C(27)−N(17)−N(18)−C(28) and C(28)−N(18)−N(17)−C(27) were 0.5. Selected bond lengths and angles are listed in Supporting Information, Table S3. All of the Fe−N coordinate bond distances (2.147(3)−2.245(12) Å) are typical for HS Fe^{II} in accordance with the magnetic study.[22] The crystal structure is shown in Supporting Information, Figure S8. The imidazole N(1)−H(4), N(6)−H(9), N(7)−H(16), and N(14)−H(23) groups of the complex containing Fe(1) are hydrogen bonded to O(1), O(6), O(8), O(9), and O(10) of ClO_4^- with distances of N(1)···O(1) = 2.971(6), N(6)···O(8) = 3.089(5), N(6)···O(9) = 3.106(6), N(7)···O(10) = 3.140(5), N(7)···O(10) = 3.008(4), and N(14)···O(6) = 2.915(4) Å. The imidazole N(15)−H(30) group of the complex containing Fe(2) is hydrogen bonded to O(2) of ClO_4^- with the distance of N(15)···O(2) = 3.061(7) Å. A 3D structure is formed by these hydrogen bonds.

Figure 10 compares intramolecular steric interactions in **1H·ClO$_4$** and **1Me·ClO$_4$**. In **1Me·ClO$_4$**, one of the azine moieties of the complex is disordered, while **1H·ClO$_4$** suffers from disorder at both azine moieties. In Figure 10, one of the ligands of each complex cation is in the plane of the paper, and the other ligand is perpendicular to the paper. The N(2)−Fe(1)−N(7) bond of **1H·ClO$_4$** is almost linear (172.73(9)°), while the corresponding bond of **1Me·ClO$_4$** is bent (161.29(11)°), and the latter is attributable to the steric effect of the methyl group. The least-squares plane (P_L) of the $H_2L^{2\text{-}Me}$ ligand (or the H_2L^H ligand), which is perpendicular to the paper, and the angles between P_L and Fe(1)−N(2) and Fe(1)−N(7) or Fe(1)−N(5) were defined as in Figure 10. The angle between P_L and Fe(1)−N(5) for **1Me·ClO$_4$** (107.3(2)°) is much larger than the corresponding angle between P_L and Fe(1)−N(2) for **1H·ClO$_4$** (95.6(6)°) because of steric effects. To cope with the steric crowding, the $H_2L^{2\text{-}Me}$ ligand deviates from planarity as evidenced by Figure 10 (b). Such steric crowding will lengthen the Fe−N bond, resulting in the HS state. Thus, the unusual order in ligand field strength, $H_2L^H > H_2L^{2\text{-}Me}$, in the mononuclear complexes can be accounted for by steric effects.

Structure of $[Fe(H_2L^{5\text{-}Me})_2](ClO_4)_2 \cdot H_2O$ (1Me′·ClO$_4$). Magnetic studies revealed that **1Me′·ClO$_4$** stays in the LS state over the temperature range 5−300 K, and the crystal structure was determined at 163 K by the X-ray diffraction method. The complex crystallizes in the space group

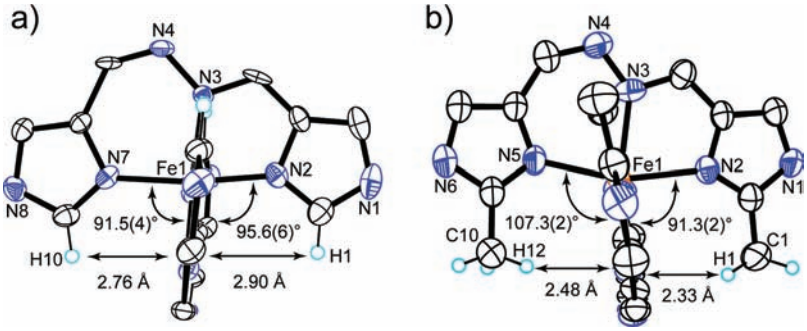

Figure 10. Comparison of the intramolecular steric interactions in (a) $[Fe(H_2L^{H})_2](ClO_4)_2\cdot 2CH_3CN$ (**1H·ClO$_4$**) and (b) $[Fe(H_2L^{2\text{-}Me})_2](ClO_4)_2\cdot 1.6CH_3CN$ (**1Me·ClO$_4$**). Severe steric repulsion exists between a methyl group of a $H_2L^{2\text{-}Me}$ ligand and the other $H_2L^{2\text{-}Me}$ ligand in **1Me·ClO$_4$**.

Table 4. Relevant Bond Lengths (Å) and Angles (deg) with Their Estimated Standard Deviations in Parentheses for $[Fe_2(H_2L^{H})_3](ClO_4)_4\cdot 5CH_3NO_2$ (**2H·ClO$_4$**) at 103 and 293 K

Bond Distances (Å)					
Fe−N(imidazole)			Fe−N(azine)		
	293 K	103 K		293 K	103 K
Fe(1)−N(2)	2.116(2)	1.979(3)	Fe(1)−N(3)	2.187(2)	1.971(3)
Fe(1)−N(8)	2.116(2)	1.972(3)	Fe(1)−N(9)	2.177(2)	1.972(2)
Fe(1)−N(14)	2.122(2)	1.979(2)	Fe(1)−N(15)	2.196(2)	1.977(3)
Fe(2)−N(4)	2.238(2)	2.215(3)	Fe(2)−N(5)	2.142(2)	2.150(3)
Fe(2)−N(10)	2.238(2)	2.221(3)	Fe(2)−N(11)	2.151(2)	2.157(2)
Fe(2)−N(16)	2.238(2)	2.218(3)	Fe(2)−N(17)	2.175(2)	2.174(3)
Fe(1)···Fe(2)	4.0362(7)	3.8507(8)			

Bond Angles (deg)		
	293 K	103 K
N(2)−Fe(1)−N(3)	75.26(10)	80.03(13)
N(8)−Fe(1)−N(9)	75.65(10)	80.27(12)
N(14)−Fe(1)−N(15)	75.18(10)	80.07(12)
N(4)−Fe(2)−N(5)	74.33(10)	74.15(12)
N(10)−Fe(2)−N(11)	73.79(9)	73.89(11)
N(16)−Fe(2)−N(17)	74.00(9)	74.35(11)

Torsion Angles (deg)		
	293 K	103 K
C(4)−N(3)−N(4)−C(5)	63.6(3)	62.2(4)
C(12)−N(9)−N(10)−C(13)	62.7(3)	58.8(4)
C(20)−N(15)−N(16)−C(21)	51.8(3)	48.4(4)

$P2_1/n$ (No. 14) with $Z = 4$. The overall molecular structure (Supporting Information, Figure S9) is similar to that of **1H·ClO$_4$**. All the Fe−N coordinate bond distances (1.942(2)−1.989(12) Å) are typical for LS Fe^{II} in accordance with the magnetic studies.

Structure of $[Fe_2(H_2L^{H})_3](ClO_4)_4\cdot 5CH_3NO_2$ (2H·ClO$_4$). Because **2H·ClO$_4$** shows SCO around 240 K, the X-ray crystal structure analysis was carried out at two temperatures, 103 and 293 K.[14] The crystallographic data are summarized in Table 2. The same space group, $P2_1/c$ (No. 14) is retained at both temperatures. Selected bond lengths and angles are collated in Table 4. Figure 11 shows an ORTEP drawing of **2H·ClO$_4$** at 293 K, with the atom numbering scheme. The structure is a dinuclear triple-helicate, with each ligand bound as a bis(bidentate) ligand to two different iron centers. Each Fe^{II} center binds to three ligand strands to attain a pseudo-octahedral coordination geometry. Each complex is chiral, with either a Δ (clockwise) or a Λ (anticlockwise) configuration because of the screw coordination arrangement of the three ligands around Fe^{II}. Both iron centers shown in Figure 11 have the Λ configuration, and thus this is a homochiral Λ−Λ pair. Because the complex crystallizes in a centrosymmetric space group $P2_1/c$, molecules with the Δ−Δ and Λ−Λ pairs coexist in the crystal to form a racemic crystal. In other words, **2H·ClO$_4$** does not undergo spontaneous resolution. All of the Fe−N coordinate bond distances (2.116(2)−2.238(2) Å) are in the range for HS Fe^{II}. The two iron centers, Fe(1) and Fe(2), are in different environments. The average Fe(1)−N bond length (2.153 Å) is smaller than that of Fe(2)−N (2.197 Å) at 293 K.

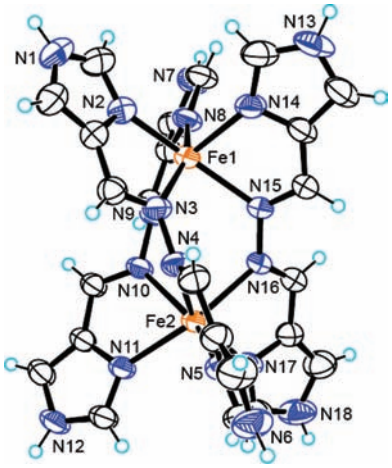

Figure 11. X-ray molecular structure of the cation of $[Fe_2(H_2L^H)_3]$-$(ClO_4)_4 \cdot 5CH_3NO_2$ (**2H·ClO$_4$**) at 293 K with an atom numbering scheme showing the 50% probability ellipsoids. Color code: orange, HS Fe; blue, N; black, C; light blue, H.

At 103 K, the average Fe(1)−N bond length (1.975 Å) is shorter by 0.178 Å than that at 293 K (2.153 Å), demonstrating that the SCO occurs at the Fe(1) site, while the Fe(2) site remains in the HS state (average Fe(2)−N bond length = 2.189 Å), to form a mixed-spin state [LS−HS] complex. The N−Fe(1)−N five-membered chelate angles (average angle = 80.12°) are larger than the N−Fe(2)−N angles (average angle = 74.13°), and the octahedron is markedly less distorted at the LS Fe(1) site than at the HS Fe(2) site. The intraligand dihedral angles between the two imidazolylimine groups decrease with decreasing temperature from 50.5(1), 53.2(1), and 41.5(1)° at 293 K to 47.4(2), 47.6(1), and 38.1(2)° at 103 K. The Fe(1)···Fe(2) distance decreases from 4.0362(7) Å at 293 K to 3.8507(8) Å at 103 K. The unit cell volume of 5610.1(3) Å^3 at 293 K decreases to 5344.3(5) Å^3 at 103 K (4.7%).

Close inspection of the crystal structures at two different temperatures suggests a factor that stabilizes the [LS−HS] state. The dinuclear complex is linked to a neighboring dinuclear unit by hydrogen bonds to form a zigzag 1D structure along the *c*-axis (Figure 12). Fe1 and Fe2 are in different environments and the two neighboring Fe1 sites are effectively linked by hydrogen bonds. In a previous paper, we showed that the effect of hydrogen bonds is similar to that of ligand deprotonation: it stabilizes the LS state.[5f] Thus, Fe1 tends to assume the LS state and the mixed-spin [LS−HS] state is stabilized.

Structure of $[Fe_2(H_2L^{2\text{-}Me})_3](ClO_4)_4$ (2Me·ClO$_4$). The temperature dependence of the magnetic susceptibility of **2Me·ClO$_4$** demonstrated that the complex stays in the LS state over the temperature range 5−300 K, and X-ray structure analysis was carried out at 293 K. Supporting Information, Figure S10 shows the molecular structure of the complex cation with the atom numbering scheme. The complex assumes a triple helicate structure as $[Fe_2(H_2L^H)_3]^{4+}$. The Fe−N coordinate bond distances (1.936(2) and 1.989(2) Å, Supporting Information, Table S4) are typical for LS Fe^{II}, and the average (1.963 Å) is close to that of the LS site for **2H·ClO$_4$** at 103 K (1.975 Å). The N−Fe(1)−N five-membered chelate angle (79.94°) is also close to that of the average (80.12°) for

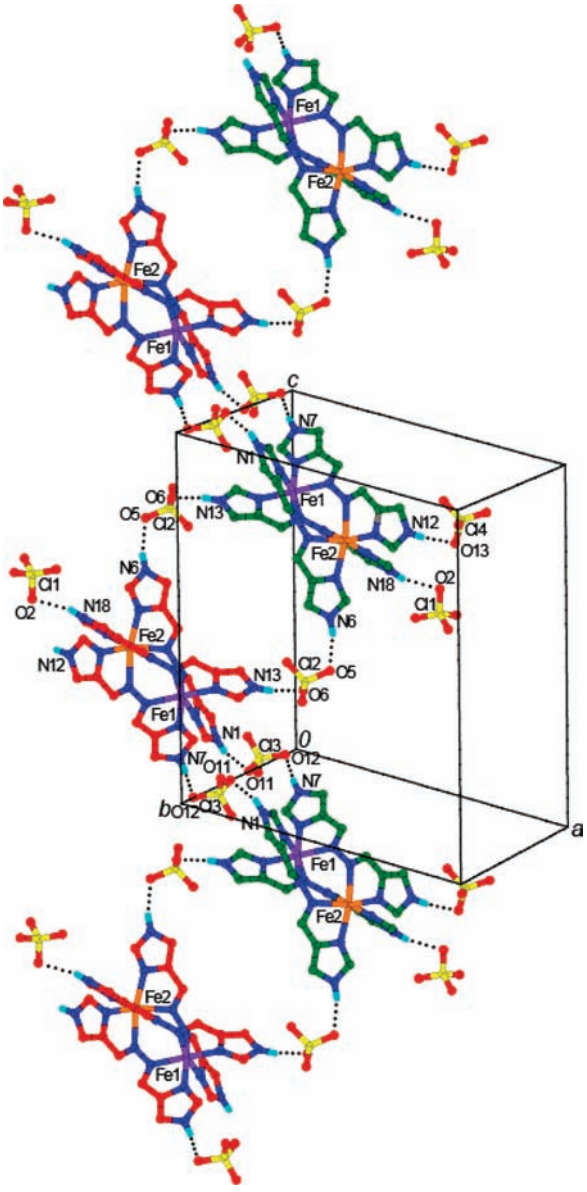

Figure 12. Crystal structure of $[Fe_2(H_2L^H)_3](ClO_4)_4 \cdot 5MeNO_2$ (**2H·ClO$_4$**) at 103 K, with a selected atom numbering scheme. Perchlorate anions and solvent molecules not participating in hydrogen bonding have been omitted for clarity. Color code: orange, HS Fe; purple, LS Fe; blue, N; light blue, H; yellow, Cl; red, O. The red and green colored molecules denote the Λ−Λ and Δ−Δ pair, respectively.

the LS site for **2H·ClO$_4$** at 103 K. The Fe(LS)···Fe(LS) distance (3.4842(7) Å) is much smaller than the Fe(LS)···Fe(HS) distance (3.8507(8) Å) for **2H·ClO$_4$** at 103 K. Unlike the mononuclear complex $[Fe(H_2L^{2\text{-}Me})_2](ClO_4)_2 \cdot 1.6CH_3CN$ (**1Me·ClO$_4$**), **2Me·ClO$_4$** involves no significant intramolecular steric repulsion between the methyl groups of an $H_2L^{2\text{-}Me}$ ligand and the other ligands. The $H_2L^{2\text{-}Me}$ ligand involving an electron-donating methyl group on each imidazole group exerts greater ligand field strength than the H_2L^H ligand. Thus, **2Me·ClO$_4$** is in the LS state even at room temperature. The crystal packing diagrams of **2Me·ClO$_4$** are shown in Supporting Information, Figure S11. The Λ−Λ pair and the Δ−Δ pair stack alternately along the *c*-axis (Supporting Information, Figure S11 (a)). There is no intermolecular interaction between the ions.

Structure of the Block Crystal of $[Fe_2(H_2L^H)_3](BF_4)_4 \cdot 6.5CH_3NO_2 \cdot 0.5H_2O$ ($2H \cdot BF_4$). As described above, when $[Fe_2(H_2L^H)_3](BF_4)_4$ ($2H \cdot BF_4$) was crystallized from nitromethane by slow diffusion of diethyl ether, two kinds of crystals (polymorphs), needles and blocks, were obtained, and they were separated manually under the microscope. We determined the structure of the block crystals by X-ray diffraction. The crystals were extremely effluorescent, and high-quality diffraction data were not available. However, we could analyze the structure to provide necessary information. The block crystals exhibited an abrupt spin transition at about 190 K, and we determined the structure at 180 K. The complex crystallizes in the space group $P\bar{1}$ (No. 2). The asymmetric unit consists of one $[Fe_2(H_2L^H)_3]^{4+}$ cation, four BF_4^- anions, and 6.5 nitromethane and 0.5 water molecules. Supporting Information, Figure S12 shows the molecular structure of the complex cation with the atom numbering scheme, and selected bond lengths and angles are collated in Supporting Information, Table S5. The complex assumes a mixed-spin [LS−HS] state at 180 K, and thus the molecular structure is similar to that of $[Fe_2(H_2L^H)_3](ClO_4)_4 \cdot 5CH_3NO_2$ ($2H \cdot ClO_4$) at 103 K, which also has a mixed-spin [LS−HS] state. The Fe(1)−N bond lengths (1.965(2)−1.987(3) Å) and Fe(2)−N bond lengths (2.144(3)−2.247(6) Å) are typical for LS Fe^{II} and HS Fe^{II}, respectively. The N(imidazole)−Fe(1)−N(azine) five-membered chelate angles (79.56−79.76°) are larger than the N(imidazole)−Fe(2)−N(azine) angles (73.24−74.19°), and the octahedron is markedly less distorted at the LS Fe(1) site than at the HS Fe(2) site. The crystal packing diagrams of $2H \cdot BF_4$ are shown in Supporting Information, Figure S13. Supporting Information, Figure S13(a) shows that all six imidazole N−H groups of a $[Fe_2(H_2L^H)_3]^{4+}$ complex cation, N(1)−H(2), N(6)−H(7), N(7)−H(10), N(12)−H(15), N(13)−H(18), and N(18)−H(23), are connected to the BF_4^- anions by hydrogen bonds to form a homochiral 2D sheet structure in the *ab*-plane. The hydrogen-bonding schemes around the two SCO sites are different, in harmony with the different SCO behaviors. All of the complex cations shown in Supporting Information, Figure S13(a) are Δ−Δ pairs. Sheets with Λ−Λ and Δ−Δ pairs stack alternately along the *c*-axis (Supporting Information, Figure S13(b)).

It is well established that the elastic interaction between SCO sites within a crystal lattice is the predominant factor governing cooperativity. The abrupt spin transition accompanied by hysteresis (Figure 7) observed for the block crystals of $2H \cdot BF_4$ may be accounted for by the 2D sheet structure involving strong intermolecular interactions.

Conclusion

Imidazole-4-carbaldehyde azine and its derivatives, H_2L^R (R = H, 2-Me, 5-Me), were prepared by condensation of 4-formylimidazole, or its derivatives, 2-methyl- or 5-methyl-4-formylimidazole, with hydrazine in a 2:1 mol ratio in methanol. The H_2L^R ligands are imidazole analogues of PAA (2-pyridinealdazine). The H_2L^R ligands afforded mononuclear $[Fe(H_2L^R)_2]^{2+}$ and dinuclear triple-helicate $[Fe_2(H_2L^R)_3]^{4+}$ complexes, and their magnetostructural relationships were studied. In contrast to $[Fe(PAA)_2]^{2+}$ and $[Fe_2(PAA)_3]^{4+}$, both of which are in the LS state, the H_2L^R complexes showed a variety of magnetic behaviors depending on such factors as the nuclearity, the kind of substituents, and counterions. When a hydrogen atom at the 2-position of imidazole in H_2L^H is replaced by an electron-donating methyl group, the ligand field strength becomes stronger and the complex tends to assume the LS state. This trend was observed in the dinuclear complexes; $[Fe_2(H_2L^H)_3]^{4+}$ and $[Fe_2(H_2L^{2\text{-Me}})_3]^{4+}$ assume the [HS−HS] and [LS−LS] spin states, respectively, at room temperature. However, the mononuclear Fe^{II} complexes, $[Fe(H_2L^H)_2]^{2+}$ and $[Fe(H_2L^{2\text{-Me}})_2]^{2+}$, afforded a different order of ligand field strengths; $[Fe(H_2L^H)_2]^{2+}$ is in the LS state while $[Fe(H_2L^{2\text{-Me}})_2]^{2+}$ is in the HS state at room temperature. X-ray structural studies revealed that the interligand steric repulsion between a methyl group of an $H_2L^{2\text{-Me}}$ ligand and the other ligand in $[Fe(H_2L^{2\text{-Me}})_2]^{2+}$ is responsible for the observed change in the spin state. In this case, the steric effect outweighs the electron-donating effect of the methyl group. $[Fe_2(H_2L^H)_3]X_4$ (X = ClO_4, BF_4) exhibited a sharp spin transition, [LS−HS] ↔ [HS−HS], and the existence of the mixed spin state [LS−HS] was confirmed from X-ray crystallographic data. The uncoordinated NH groups of the imidazole moiety of $[Fe_2(H_2L^R)_3]^{4+}$ can be partly deprotonated to form intermolecular N−H···N hydrogen bonds. Because the dinuclear complexes have a homochiral structure, Δ−Δ or Λ−Λ, controlled deprotonation of $[Fe_2(H_2L^R)_3]^{4+}$ may form a homochiral SCO complex with high dimensionality. Studies along this line are in progress in our laboratories.

Experimental Section

Caution! *Perchlorate salts of metal complexes are potentially explosive. Only small quantities of material should be prepared and the samples should be handled with care.*

Materials. All reagents and solvents used in the syntheses were of reagent grade and they were used without further purification.

Ligands, H_2L, $H_2L^{2\text{-Me}}$, and $H_2L^{5\text{-Me}}$. The H_2L^H (= imidazole-4-carbaldehyde azine), $H_2L^{2\text{-Me}}$ (= 2-methylimidazole-4-carbaldehyde azine), and $H_2L^{5\text{-Me}}$ (= 5-methylimidazole-4-carbaldehyde azine) ligands were prepared by condensation of hydrazine and 4-formylimidazole or 2-methyl- or 5-methyl-4-formylimidazole in a 1:2 mol ratio in methanol. The representative method is given for H_2L^H. A methanol solution (10 mL) of hydrazine monohydrate (1.75 g, 35 mmol) was added to a warm methanol solution (90 mL) of 4-formylimidazole (6.71 g, 70 mmol). The mixture was stirred for 1 h, and a pale yellow precipitate was collected by filtration. **H_2L^H**: Yield: 5.68 g (86%). Anal. Found: C, 51.14; H, 4.09; N, 44.62%. Calcd for $C_8H_8N_6$: C, 51.06; H, 4.28; N, 44.66%. IR (KBr disk): $\nu_{C=N}$ (imine) 1639 cm^{-1}.

$H_2L^{2\text{-Me}}$: Yield: 79%. Anal. Found: C, 55.46; H, 5.51; N, 38.69%. Calcd for $C_{10}H_{12}N_6$: C, 55.54; H, 5.59; N, 38.86%. IR (KBr disk): $\nu_{C=N}$ (imine) 1638 cm^{-1}. Crystals suitable for the X-ray structure analysis were obtained by slow evaporation of the filtrate.

$H_2L^{5\text{-Me}}$: Yield: 74%. Anal. Found: C, 55.29; H, 5.26; N, 38.54%. Calcd for $C_{10}H_{12}N_6$: C, 55.54; H, 5.59; N, 38.86%. IR (KBr disk): $\nu_{C=N}$ (imine) 1637 cm^{-1}.

$[Fe(H_2L^H)_2](ClO_4)_2 \cdot CH_3OH$ ($1H \cdot ClO_4$). $Fe(ClO_4)_2 \cdot 6H_2O$ (0.363 g, 1.0 mmol) was added to a suspension of H_2L^H (0.376 g, 2.0 mmol) in methanol (20 mL). The color of the mixture changed from reddish orange to purple on heating at 60 °C for 1 h. The solution was filtered, and diethyl ether (60 mL) was added to the filtrate. Dark purple crystals deposited on standing

in a refrigerator were collected by filtration. Yield: 66%. Anal. Found: C, 30.74; H, 2.88; N, 25.13%. Calcd for $C_{17}H_{20}Cl_2FeN_{12}O_9$: C, 30.79; H, 3.04; N, 25.34%. IR (KBr disk): $\nu_{C=N}$ (imine) 1622, 1588 cm^{-1}; ν_{Cl-O} (ClO_4^-) 1143, 1088 cm^{-1}. Crystals suitable for the X-ray structure analysis ($[Fe(H_2L^H)_2](ClO_4)_2 \cdot 2CH_3CN$) were obtained by recrystallization from acetonitrile−toluene.

$[Fe(H_2L^{2\text{-}Me})_2](ClO_4)_2 \cdot H_2O$ (1Me·ClO_4). This complex was prepared by the same method as for **1H·ClO_4** except that $H_2L^{2\text{-}Me}$ was used instead of H_2L^H, and the complex was obtained as dark red crystals. Yield: 92%. Anal. Found: C, 34.12; H, 3.74; N, 23.53%. Calcd for $C_{20}H_{26}Cl_2FeN_{12}O_9$: C, 34.06; H, 3.72; N, 23.83%. IR (KBr disk): $\nu_{C=N}$ (imine) 1630, 1594 cm^{-1}; ν_{Cl-O} (ClO_4^-) 1118, 1088 cm^{-1}. Crystals suitable for the X-ray structure analysis ($[Fe(H_2L^{2\text{-}Me})_2](ClO_4)_2 \cdot 1.6CH_3CN$) were obtained by diffusion of diisopropyl ether to an acetonitrile solution of the complex.

$[Fe(H_2L^{5\text{-}Me})_2](ClO_4)_2 \cdot 1.5H_2O$ (1Me′·ClO_4). This complex was prepared by the same method as for **1H·ClO_4** except that $H_2L^{5\text{-}Me}$ was used instead of H_2L^H, and the complex was obtained as purple crystals. Yield: 78%. Anal. Found: C, 33.70; H, 3.71; N, 23.29%. Calcd for $C_{20}H_{27}Cl_2FeN_{12}O_{9.5}$: C, 33.63; H, 3.81; N, 23.59%. IR (KBr disk): $\nu_{C=N}$ (imine) 1628, 1568 cm^{-1}; ν_{Cl-O} (ClO_4^-) 1087 cm^{-1}.

$[Fe_2(H_2L^H)_3](ClO_4)_4$ (2H·ClO_4). $Fe(ClO_4)_2 \cdot 6H_2O$ (0.726 g, 2.0 mmol) was added to a suspension of H_2L^H (0.564 g, 3.0 mmol) in nitromethane (30 mL), and the mixture was stirred in an ice-bath for 2 h. The reaction mixture was filtered to remove any undissolved substance, and diethyl ether (60 mL) was added to the filtrate to form orange crystals. Yield: 0.603 g (56%). Anal. Found: C, 27.00; H, 2.38; N, 23.11%. Calcd for $C_{24}H_{24}Cl_4Fe_2N_{18}O_{16}$: C, 26.83; H, 2.25; N, 23.47%. IR (KBr disk): $\nu_{C=N}$ (imine) 1629 cm^{-1}; ν_{Cl-O} (ClO_4^-) 1144, 1118, 1088 cm^{-1}.

$[Fe_2(H_2L^{2\text{-}Me})_3](ClO_4)_4$ (2Me·ClO_4). This complex was prepared by the same method as for **2H·ClO_4** except that $H_2L^{2\text{-}Me}$ was used instead of H_2L^H, and the complex was obtained as dark brown crystals. Yield: 80%. Anal. Found: C, 30.78; H, 3.03; N, 21.43%. Calcd for $C_{30}H_{36}Cl_4Fe_2N_{18}O_{16}$: C, 31.14; H, 3.13; N, 21.76%. IR (KBr disk): $\nu_{C=N}$ (imine) 1617 cm^{-1}; ν_{Cl-O} (ClO_4^-) 1111 cm^{-1}.

$[Fe_2(H_2L^{5\text{-}Me})_3](ClO_4)_4$ (2Me′·ClO_4). This complex was prepared by the same method as for **2H·ClO_4** except that $H_2L^{5\text{-}Me}$ was used instead of H_2L^H, and the complex was obtained as reddish brown crystals. Yield: 20%. Anal. Found: C, 31.29; H, 3.46; N, 21.75%. Calcd for $C_{30}H_{36}Cl_4Fe_2N_{18}O_{16}$: C, 31.14; H, 3.13; N, 21.76%. IR (KBr disk): $\nu_{C=N}$ (imine) 1634 cm^{-1}; ν_{Cl-O} (ClO_4^-) 1088 cm^{-1}.

$[Fe_2(H_2L^H)_3](BF_4)_4$ (2H·BF_4). $Fe(BF_4)_2 \cdot 6H_2O$ (0.450 g, 1.33 mmol) was added to a suspension of H_2L^H (0.376 g, 2.0 mmol) in nitromethane (20 mL), and the mixture was stirred in an ice bath for 30 min. The reaction mixture was filtered to remove any undissolved substance, and diethyl ether (60 mL) was added to the filtrate to form two kinds, block and needle, crystals. Yield: 0.40 g (59%). They were separated manually.

Needle Crystals. Anal. Found: C, 28.13; H, 2.20; N, 24.21%. Calcd for $C_{24}H_{24}B_4F_{16}Fe_2N_{18}$: C, 28.16; H, 2.36; N, 24.63%.

Block Crystals. Anal. Found: C, 28.22; H, 2.03; N, 24.54%. Calcd for $C_{24}H_{24}B_4F_{16}Fe_2N_{18}$: C, 28.16; H, 2.36; N, 24.63%. IR (KBr disk): $\nu_{C=N}$ (imine) 1628 cm^{-1}; ν_{B-F} (BF_4^-) 1118, 1084, 1039 cm^{-1}. Diffusion of diisopropyl ether to a nitromethane solution of the complex also yielded a mixture of needle crystals and block crystals, and the block crystals were suitable for the X-ray structure analysis.

Physical Measurements. Elemental analyses (C, H, N) were performed on a Perkin-Elmer 2400II elemental analyzer. IR spectra were recorded on a JASCO FT/IR FT-550 spectrophotometer with the samples prepared as KBr disks. UV−visible absorption spectra were recorded with a JASCO Ubest-550 spectrophotometer. Cyclic voltammetry measurements were performed using a Fuso HECS 321B potential sweep unit with acetonitrile solutions containing $(n\text{-}Bu)_4NBF_4$ (0.1 M) as supporting electrolyte. The electrochemical cell was a three-electrode system consisting of a glassy carbon working electrode, a platinum wire auxiliary electrode, and an Ag/Ag^+ (Ag/0.01 M $AgNO_3$) reference electrode. As an external standard, the Fc/Fc^+ (Fc = ferrocene) couple was observed at +0.077 V versus Ag/Ag^+ under the same conditions. Differential scanning calorimetry (DSC) measurements were performed with a Perkin-Elmer Pyris 1. The samples were located in sealed samples pans, and the DSC profiles were recorded at a rate of 5 K min^{-1}. Magnetic susceptibilities were measured with a Quantum Design MPMS SQUID magnetometer in the 5−300 K temperature range at 2 K min^{-1} sweep rate under an applied magnetic field of 1 T. Corrections for diamagnetism were applied using Pascal's constants. The Mössbauer spectra were recorded by using a Wissel 1200 spectrometer and a proportional counter. ^{57}Co-(Rh), moving in a constant acceleration mode, was used as the radioactive source. The hyperfine parameters were obtained by least-squares fitting to Lorentzian peaks. The isomer shifts are reported relative to metal iron foil at 293 K. The sample temperature was controlled by a Heli-tran liquid transfer refrigerator (Air Products and Chemicals, Inc.) with an accuracy of ± 0.5 K.

X-ray Data Collection, Reduction, and Structure Determination. The X-ray data were collected using a Rigaku RAXIS RAPID II imaging plate area detector employing graphite monochromated Mo Kα radiation (λ = 0.71073 Å). The structures were determined by direct methods (SHELXS 97 or SIR97[23]) and expanded using Fourier techniques[24] and successive Fourier difference methods with refinement of full matrix least-squares on F^2. The non-hydrogen atoms were refined anisotropically. Hydrogen atoms were introduced in calculations using the riding model. All calculations were performed using the Crystal Structure 3.8 software package.[25] Disorders were treated using SHELXL 97.

Acknowledgment. This work was supported in part by a Grant-in-Aid for Scientific Research (Nos. 16205010, 17350028, and 20550064) from the Ministry of Education, Science, Sports, and Culture of Japan, and by the Iketani Science and Technology Foundation.

Supporting Information Available: X-ray crystallographic files in CIF format for compounds $H_2L^{2\text{-}Me}$, **1H·ClO_4**, **1Me·ClO_4**, **1Me′·ClO_4**, **2Me·ClO_4**, and **2H·BF_4**. Table of Mössbauer spectral parameters for **2H·ClO_4**. Tables of selected bond lengths and angles for $H_2L^{2\text{-}Me}$, **1Me·ClO_4**, **2Me·ClO_4**, and **2H·BF_4**. Cyclic voltammograms of **2H** and **2Me**. Magnetic behaviors of **2H·BF_4**. DSC for the needle crystals and block crystals of **2H·BF_4**. X-ray molecular structures of **1Me·ClO_4**, **1Me′·ClO_4**, **2Me·ClO_4**, and **2H·BF_4**. X-ray crystal structures of $H_2L^{2\text{-}Me}$, **1H·ClO_4**, **1Me·ClO_4**, **2Me·ClO_4**, and **2H·BF_4**. This material is available free of charge via the Internet at http://pubs.acs.org. X-ray crystallographic data are also available from Cambridge Crystallographic Data Centre at the deposit numbers CCDC738548−738553.

(23) Sheldrick, G. M. *SHELX 97*; University of Göttingen: Göttingen, Germany, 1997.SIR97; Altomare, A.; Burla, M.; Moliterni, A.; Polidori, G.; Spagna, R. *J. Appl. Crystallogr.* **1999**, *32*, 115–119.

(24) Beurskens, P. T.; Admiraal, G.; Beurskens, G.; Bosman, W. P.; Gelder, de R.; Israel, R. ; Smits, J. M. M. *DIRDIF99: The DIRDIF-99 program system, Technical Report of the Crystallography Laboratory*; University of Nijmegen: The Netherlands, 1999.

(25) *CrystalStructure 3.8; Crystal Structure Analysis Package*; Rigaku and Rigaku/MSC: The Woodlands, TX, 2001−2007.